Article

An Electrical Inspection of the Subsurface Cisternae of the Outer Hair Cell

Lei Song[1] and Joseph Santos-Sacchi[1,2,3,*]
[1]Surgery (Otolaryngology), [2]Neurobiology, and [3]Cellular and Molecular Physiology, Yale University School of Medicine, New Haven, Connecticut

ABSTRACT The cylindrical outer hair cell (OHC) of Corti's organ drives cochlear amplification by a voltage-dependent activation of the molecular motor, prestin (SLC26a5), in the cell's lateral membrane. The voltage-dependent nature of this process leads to the troublesome observation that the membrane resistor-capacitor filter could limit high-frequency acoustic activation of the motor. Based on cable theory, the unique 30 nm width compartment (the extracisternal space, ECS) formed between the cell's lateral membrane and adjacent subsurface cisternae (SSC) could further limit the influence of receptor currents on lateral membrane voltage. Here, we use dual perforated/whole-cell and loose patch clamp on isolated OHCs to sequentially record currents resulting from excitation at apical, middle, and basal loose patch sites before and after perforated patch rupture. We find that timing of currents is fast and uniform before whole-cell pipette washout, suggesting little voltage attenuation along the length of the lateral membrane. Prior treatment with salicylate, a disrupter of the SSC, confirms the influence of the SSC on current spread. Finally, a cable model of the OHC, which can match our data, indicates that the SSC poses a minimal barrier to current flow across it, thereby facilitating rapid delivery of voltage excitation to the prestin-embedded lateral membrane.

INTRODUCTION

The outer hair cell (OHC) provides a unique function for mammalian hearing, underlying a 40–60 decibel boost that enhances our ability to detect and discriminate among sounds, namely, cochlear amplification (1). The structure of the OHC is likewise unique, being cylindrical and ranging in length over tens of micrometers depending on tonotopic location along the cochlea spiral, reaching ~90 μm in the apical OHC of the guinea pig. The lateral wall of the OHC, composed of the lateral plasma membrane, cortical cytoskeleton, and subsurface cisternae (SSC), hosts a restricted subplasmalemmal compartment of 30–50 nm width, termed the extra cisternal space (ECS) (2,3). This ECS is an interesting compartment because prestin, the molecular motor that drives OHC electromotility, resides in the adjacent plasma membrane, with its C- and N-terminals and its anion-binding site projecting into the space (4–6). Prestin contributes to the lateral membrane's capacitance, not only linearly, due to its abundant occupancy increasing surface area (7,8), but nonlinearly because of the electrical signature of prestin activity, namely, nonlinear capacitance (NLC) (9,10). Previous modeling efforts have attributed special electrical characteristics to the ECS (11,12), but they did not include NLC in the lateral plasma membrane.

One recurring concern with the voltage-dependent nature of OHC electromotility is the membrane resistor-capacitor (RC) filter effect on the driving force (sound-induced receptor potentials) for prestin activation. Indeed, it has been estimated that OHC mechanical responses would be 20 dB less than basilar membrane movements at high acoustic frequencies (13). Since then, a number of solutions to the RC problem have been proposed, in an attempt to confirm high frequency, cycle-by-cycle voltage drive for the cochlea amplifier. The presence of the SSC/ECS might also interfere with voltage delivery to the lateral membrane, presenting barriers to receptor current flow. In this report, we directly investigate the influence of the SSC/ECS on OHC electrical behavior. Using dual voltage clamp on isolated OHCs, we find that whole-cell recording via perforated patch records equally fast responses from electrical stimulation of the lateral membrane along its entire length via loose patch. Cable modeling indicates that the SSC barrier does not limit current spread to the ECS, thereby facilitating efficient and rapid delivery of voltage drive to the molecular motors within the lateral membrane.

MATERIALS AND METHODS

Experiment

Electrical measurements were made with modifications to the approach used by Anson and Roberts (14). Three types of electrode arrangements were used—perforated patch whole-cell recording followed by patch rupture into standard whole-cell mode, each accompanied by roving loose patch voltage stimulation. Specifically, two electrodes were patched onto isolated OHCs simultaneously: a perforated patch electrode (gramicidin, 25 or 50 μg/ml) initially served as the recording electrode (holding potential at 0 mV), and a loose patch electrode placed at three locations along the lateral membrane to deliver voltage stimulations. Subsequently, the perforated patch electrode was ruptured to make recordings under standard whole-cell mode. The perforated patch permitted replacement of

Submitted September 11, 2014, and accepted for publication December 8, 2014.

*Correspondence: joseph.santos-sacchi@yale.edu

Editor: Miriam Goodman.

0006-3495/15/02/0568/10 $2.00

http://dx.doi.org/10.1016/j.bpj.2014.12.010

intracellular cations with those of pipette cations, notably Na to inhibit K currents in the basal membrane, thus reducing their effects on our measures of currents and NLC. We view the perforated patch condition as the least intrusive and thus the condition most indicative of normal cellular behavior.

Isolated OHCs from the organ of Corti of guinea pigs were obtained as previously described (15). Long cells (~80 μm long) from apical turns were chosen to allow reliable cable analysis. We used 5 mM chloride to mimic the intracellular chloride concentration of the normal cell that we measured previously (16). Prestin is sensitive only to intracellular chloride, and to clamp intracellular chloride to 5 mM we needed to match inside and outside chloride because the lateral membrane harbors a substantial chloride conductance (6). The bath solution contained, in mM, NaCl 5, Na gluconate 135, $CaSO_4$ 2, $MgSO_4$ 1.2, and HEPES 10. Final solutions were adjusted to 300 mOsm with D-glucose and pH 7.2~7.3 with NaOH. The whole-cell patch pipette solution was the same as the extracellular solution except with the addition of 10 mM EGTA. Loose patch electrodes contained the bath solution with resistances near 1 MΩ. Loose patch electrodes served as stimulating electrodes roving along the lateral membrane of OHCs (Fig. 1), positioned ~20, 45, and 70 μm from the base of the cell. To reduce cellular adhesion to the roving pipette, tips were treated with trichlorosilane. Experiments were performed at room temperature (22–23°C). A Nikon Eclipse E600-FN microscope with 40× water immersion lens was used to observe cells during the electrical measurements.

Axon 200B amplifiers were used for patch clamping, currents being sampled at 10 μs with an Axon Digidata 1322 using jClamp software (www.scisoftco.com). Voltage steps of 20 ms duration ranging from −160 to +160 mV with 20 mV steps were delivered via a loose patch electrode. Perforated patch electrodes were used to collect current data. Recorded currents were filtered with a 10 kHz 4 pole Bessel filter. Current traces were individually fit with single exponentials in jClamp. Initial electrode resistance was 4–6 MΩ. Gigohm seals are reached before decrease of patch resistance due to gramicidin perforation. With pipette backfilling, time for establishing perforated patch whole-cell patch was around 30–40 min. R_s for the perforated patch electrode was typically 15–25 MΩ, and was reduced by series resistance compensation to maintain a ~10 MΩ resistance. Similarly, after rupture of the perforated patch and establishment of whole-cell recording, R_s was maintained near 10 MΩ. It was important to keep electrode series resistance uniform among cell recordings because time constants are dependent on the series resistance. Amplifier lag controls were not manipulated but were left at minimum levels during R_s compensation. The recording protocol (perforated patch recording with apical, middle, and basal stimulation, followed by whole-cell recording and roving stimulation) was quite demanding so that many cells were lost before completing all recording conditions. Whole-cell NLC was measured with the recording electrode using a 2-sine voltage stimulus atop a voltage ramp with subsequent admittance analysis as previously described (17).

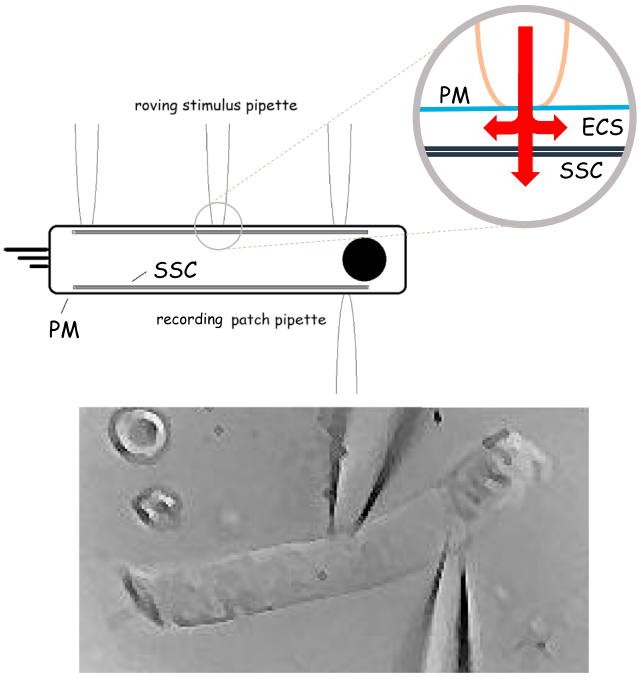

FIGURE 1 Schematic of OHC under voltage clamp with recording patch pipette, while being stimulated with a roving loose patch pipette. The enlarged section shows possible current flow from the loose patch electrode. Beneath is a digitally captured image of an OHC during middle position stimulation. To see this figure in color, go online.

To investigate the effects of subsurface cisternae damage, OHCs were incubated in extracellular solutions that contained 10 mM salicylate for 30–40 min. This time period of exposure has been shown to cause irreversible damage to the subsurface cisternae (3), thereby minimizing contributions of the SSC/ECS to our measures. Washout of salicylate was performed before recording to alleviate its direct reversible effects on prestin's NLC (18,19).

Average responses for stimulation at basal, middle, and apical positions for a range of step voltage commands included three cells where all recording/stimulation configurations were successfully completed. Statistical tests included cells where less than the full paradigm was completed, with numbers ranging from 3 to 10 (see Fig. 4 for numbers of cells used for statistical tests). We were careful to ensure that electrophysiological conditions (especially recording clamp time constants) were similar before and after patch rupture. Results for perforated/whole-cell conditions (with standard −10 mV pulse stimulation via the recording pipette) were (mean ± SE; $n = 3$): Rs: 10.1 ± 0.1 MΩ vs. 10.4 ± 0.2 MΩ; Rm: 314 ± 83 MΩ vs. 256 ± 87 MΩ; Cm 39.4 ± 1.15 pF vs. 41.8 ± 1.9 pF; clamp τ: 375 ± 12 μs vs. 403 ± 26 μs. These measures were repeated and remained stable for each roving pipette stimulation configuration. For salicylate-treated cells, perforated/whole-cell conditions were (mean ± SE; n=3): R_s: 10.5 ± 0.2 MΩ vs. 10.4 ± 0.2 MΩ; R_m: 267 ± 36 MΩ vs. 262 ± 42 MΩ; C_m 40.1 ± 0.2 pF vs. 40.0 ± 0.4 pF; clamp τ: 401 ± 9 μs vs. 395 ± 8 μs.

Model

A lumped parameter model and a cable model of 47 sections that helped to understand the data were implemented in MATLAB's Simulink (The MathWorks, Natick, MA) using Simscape and are schematized (see Figs. 5 *a* and 6 *a*). The cable model was a standard one-dimensional model similar to that of Halter et al. (11) (see Results below). Though the length of the OHCs that we modeled was short compared to typical cell lengths used for cable analyses, we found it beneficial to analyze in this manner to compare to previous results and help in defining current paths and resistances within the OHC. An automation link between jClamp and MATLAB allowed us to stimulate the model and analyze in jClamp, similar to the biophysical experiments. Parameters were taken from the biophysical data as provided in Results. Both whole-cell and loose patch NLC were modeled as

$$C_m = Q_{\max}\frac{ze}{kT}\frac{b}{(1+b)^2} + C_{lin},$$

$$b = \exp\left(\frac{-ze(V_m - V_h)}{kT}\right),$$

where $Q_{\max}$ is the maximum charge moved, z is valence, C_{lin} is the linear capacitance of the cell membrane and V_h is the voltage at half-maximal charge. E, k, and T have their usual meanings.

To fit current transients to the cable model, we averaged traces across all cells. Because the absolute magnitudes of the currents differed and we were

concerned with maintaining time constant information, we first scaled all currents to unity based on peak current, and then averaged and rescaled to average magnitude. In this way, current shapes (tau) from all traces contributed equally to the averages.

RESULTS

Experiment

We investigated longitudinal charge movement within the cell by recording with perforated patch clamp while simultaneously stimulating along the length of isolated OHCs using a loose patch electrode (Fig. 1), in a manner similar to that of Anson and Roberts (14). Perforated patch recording leaves the plasma membrane unbroken but allows electrical continuity with the whole cell (20). The enlarged, circled section in Fig. 1 indicates possible current flow from the stimulating loose patch electrode into the ECS or across the SSC into the axial core of the cell. We found that loose patch stimulation at all cell positions relative to the recording electrode produced equally fast responses under the perforated recording condition. Interestingly, we only observed single exponential responses. For example, Fig. 2, *A–C*, shows that time constants of induced current transients were similar with basal, middle, and apical stimulation during perforated patch recording conditions, regardless of voltage stimulation magnitude. These data may indicate that charge movement within and along the ECS is rapid. However, upon perforated patch rupture with suction, and establishment of standard whole-cell recording, time constants showed differences; apical and middle stimulation showed slower responses, and interestingly took on a clear voltage dependence arising from the loose patch's NLC (Fig. 2, *D–F*). We take this to indicate that the SSC was somehow altered either by washout of cell constituents or washin of gramicidin, resulting in altered characteristics of the cell's cable properties. Whole-cell NLC measured under these two conditions were similar (Fig. 2, *C* and *F*), indicating that the large increase in time constants is not due to a corresponding large increase in NLC of the whole cell. It should be noted that limiting time constants are imposed by the patch clamp (roughly, RsCm) and in absolute terms do not reflect cell capabilities. We only use these measures as a tool to understand relative timing relationships between conditions and between electrodes.

The incorporation of gramicidin into a membrane is a fairly slow process; for example, up to 45 min is required to obtain good series resistance of the perforated patch electrode before beginning our experiments. Following patch rupture, we required only ~10 min to complete the rest of the experiment, though maintaining the cell for the complete protocol was not guaranteed. Thus, little gramicidin is expected to incorporate with the plasma membrane and this is evidenced by the maintenance of fairly high membrane resistance in whole-cell mode (see Materials and Methods for values). In any case, a reduction in membrane resistance should speed up the electrical response rather than slow it down, as occurred after patch rupture. Thus, we reasoned that establishing the whole-cell condition by pipette suction caused alterations to the SSC during washout/in. To test this hypothesis, we transiently treated cells with salicylate, which has been shown to irreversibly alter SSC ultrastructure (3). The effect of prior salicylate treatment (30–45 min) was to abolish the increase in time constants that occur following patch rupture, as would be expected if the SSC/ECS were altered before patch rupture (Fig. 3, *A* and *B*). As with untreated cells, we were careful to ensure that recording conditions were similar before and after patch

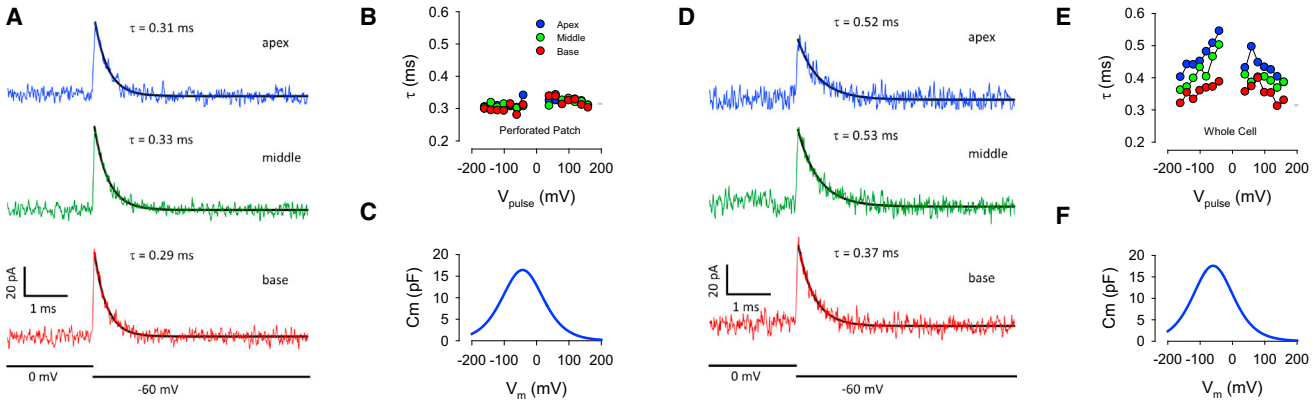

FIGURE 2 Time constants (τ) of current responses induced by step voltages of the roving loose patch electrode before (*A–C*) and after (*D–F*) rupture of recording the electrode perforated patch. (*A*) Traces of currents measured during apical, middle, and basal stimulation. Traces are averages (see Materials and Methods). Note that current responses have similar exponential decays. (*B*) Average response tau across voltage stimulation magnitude. Circles depict average responses at each voltage for 3–10 cells. (*C*) NLC based on average fits (see Materials and Methods). Q_{max}, V_h, z: 2.95 pC, −59.7 mV, 0.61. (*D*) Traces of currents measured during apical, middle, and basal stimulation following recording electrode patch rupture into standard whole-cell mode. Traces are averages. Note that current responses now have differing exponential decays. (*E*) Average response tau across voltage stimulation magnitude, showing clear voltage dependence. Circles depict average responses at each voltage. (*F*) NLC based on average fits. Q_{max}, V_h, z: 2.81 pC, −43.2 mV, 0.60. To see this figure in color, go online.

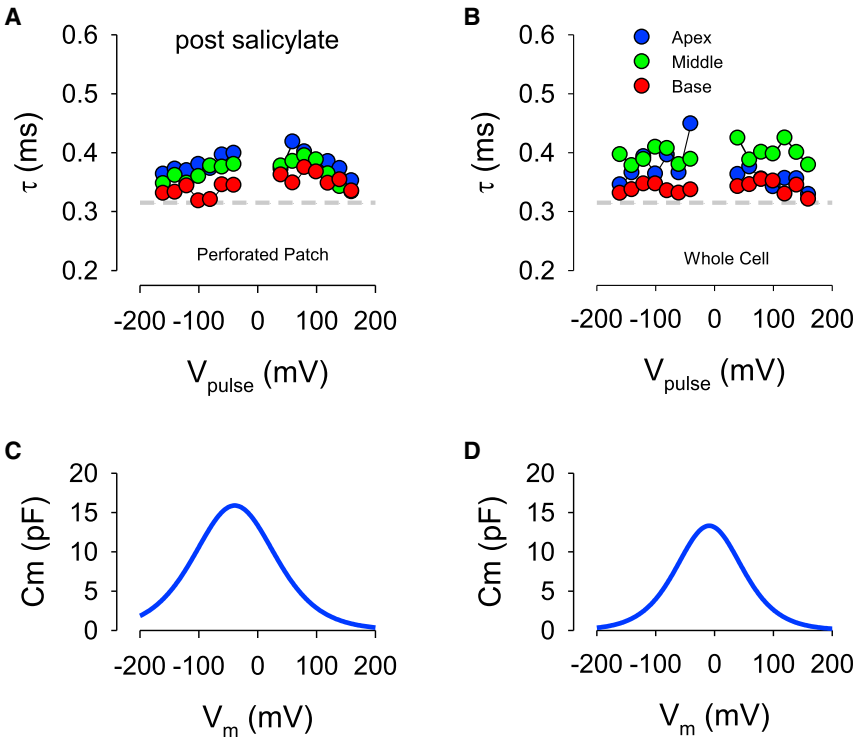

FIGURE 3 Time constants (τ) of perforated (*A*) and whole-cell (*B*) patch responses following salicylate treatment induced by step voltages of the roving loose patch electrode. Circles depict average responses at each voltage for three cells. Note similarity of time constants (τ) before and after establishment of whole-cell condition. (*C*) and (*D*) show corresponding measures of average NLC measured with whole-cell/perforated patch electrode (Q_{max}, V_h, z: 2.94/2.00 pC, −39.0/−9.2 mV, 0.55/0.68). To see this figure in color, go online.

rupture (see Materials and Methods). In these cells, NLC before patch rupture was slightly less than controls not treated with salicylate (compare Fig. 2, *C* and *F* with Fig. 3, *C* and *D*). After patch rupture, NLC was shifted rightward and decreased somewhat (see figure legends for fits).

Fig. 4, *A* and *B*, compare the time constants obtained at −60 mV steps and time to peak current (Tpk) at the 160 mV pulse, each at three locations, before and after establishing whole-cell conditions for cells without salicylate treatment. Statistically significant differences are found at all stimulation locations (significance is given in plot). The observations on current time constants are to a large extent paralleled by measures of Tpk. That is, although these metrics were stable across stimulus locations for the perforated patch condition, they increased for the whole-cell condition. For example, current spread latency between

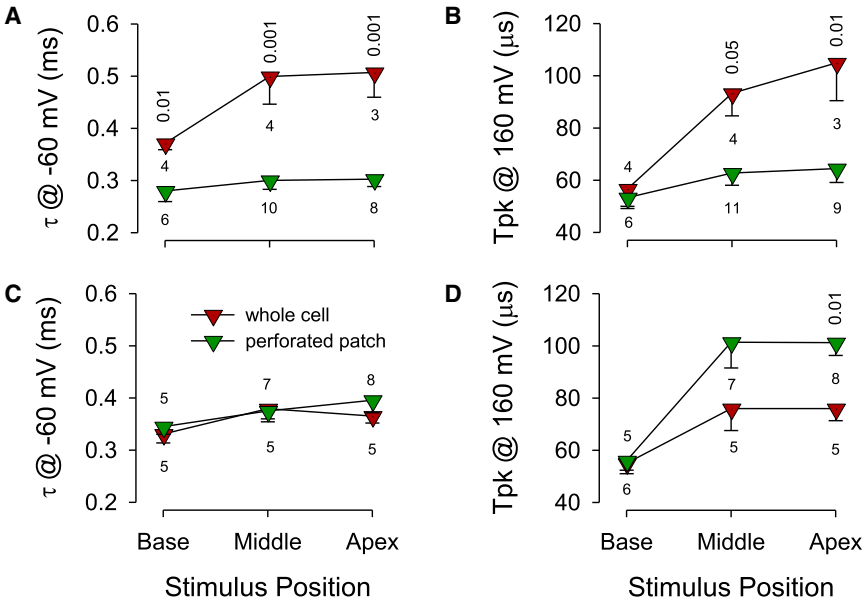

FIGURE 4 (*A*) Average time constants at −60 mV show little difference among roving patch locations for the perforated patch condition, but significant differences following whole-cell recording. (*B*) Similarly, times to peak (Tpk) current increase at apical and middle positions following patch rupture. (*C*) For salicylate-treated cells, time constants show no significant differences between perforated patch and whole-cell conditions. (*D*) Tpk shows no significant differences at basal and middle positions; however, a difference was observed at the apical position where Tpk was now shorter following patch rupture. Number of cells is noted. Statistical significance ($p <$; *t*-test), where present, between pre- and post-patch rupture is shown for each location. To see this figure in color, go online.

stimulating and recording electrodes based on Tpk between basal and apical stimulation is on the order of only 3.4 μs (53.3 +/− 3.3 vs. 56.7+/− 4.0 μs; $p > 0.05$), whereas following establishment of whole-cell conditions the spread significantly slowed to 41.1 μs (105.0 +/− 14.5 vs. 64.4 +/− 5.2 μs; $p < 0.05$). Fig. 4 *C* shows that no significant differences are found in time constants for the salicylate-treated case, indicating that SSC alterations were present both before and after patch rupture. TpK for salicylate-treated cells show no differences at basal and middle stimulation locations (Fig. 4 *D*), but a significant difference is found for the apical stimulation position. However, this difference, namely that Tpk is shortened following rupture, is opposite that observed without salicylate (see Fig. 4 *B*). This may indicate an interactive action of combined salicylate and gramicidin.

Models

Lumped parameter model

To understand our results, we constructed a lumped parameter model of the OHC, before and after establishing whole-cell configuration (Fig. 5 *A*). The model parameters are those actual averaged (see above) measures obtained in perforated patch mode (*condition 1*) and whole-cell mode (*condition 2*). C_p, the linear capacitance of the patch, and patch NLC were set to 0.02 of the measured whole-cell values. R_p, the patch resistance that was stimulated, was set based on Halter et al.'s value of lateral membrane conductivity, 0.001 mS/cm^2 (11). This is reasonable, because we have previously shown that the lateral membrane is devoid of voltage-dependent conductances (21). V_h of the loose patch was set to a 20 mV more depolarized value than whole-cell or perforated patch V_h because the tension provided to the patch (~1 kP) to increase loose patch shunt resistance (R_{sh}) is known to shift V_h ~20 mV/kP (22). R_{sh} was set to 5.0 MΩ. R_{sp} was set to 1.8 MΩ, based on measures of electrode resistance before cell attachment. Stimulation was done as with the biophysical measures using jClamp and Simulink. In the perforated condition, an intervening resistance (R_{inter}) between stimulating and recording electrodes of 10 MΩ or less produced results that resembled our data (see below).

Fig. 5 *B* shows the time constants of evoked currents when the model was simulated with parameters obtained under perforated patch and whole-cell experimental conditions. Though tau were similar in magnitude to our data, no differences in tau are observed between the two conditions, unlike the increase in voltage-dependent tau that we observed experimentally. This means that the differences observed between model and data are not due to the experimentally observed changes in R_s, R_m, C_{lin}, and NLC between the two conditions. Could unrecognized changes in R_{sp} or R_{sh} have influenced our data? In Fig. 5, *C* and *D*, we show the effects of altering R_{sp} (1, 5, 10 MΩ) and R_{sh} (1, 5, 15 MΩ). No influence on tau was found. Changes in R_{sh} can, however, alter the magnitude of the current response, and thus could underlie differences between current magnitudes found in whole-cell and perforated patch recordings. Finally, we modified R_{inter} (10, 100, 300 MΩ) and found an increase in voltage-dependent tau as a function

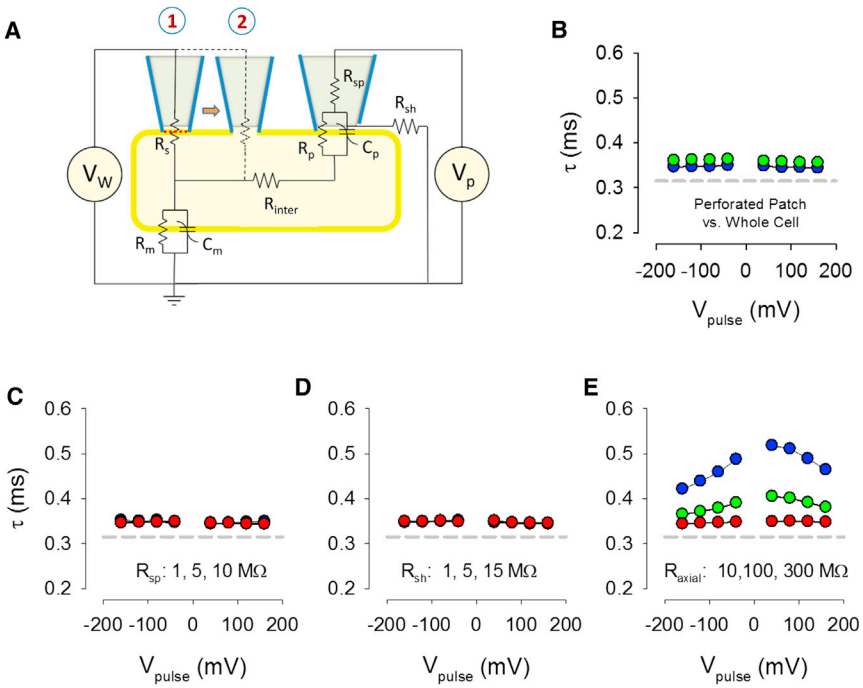

FIGURE 5 Lumped parameter model of OHC under the experimental conditions. (*A*) Schematic showing circuit and parameters of current measuring and voltage stimulating pipettes. Model was evaluated first under perforated patch (*condition 1*) and then under whole-cell (*condition 2*). See Materials and Methods for details. Right pipette is stimulating pipette. Parameters are taken from actual biophysical data given in Results. (*B*) With biophysical measures obtained under perforated patch and whole-cell condition, no differences in taus are observed. (*C* and *D*) Neither R_{sh} nor R_{sp} affects the evoked current time constants. However, interelectrode resistance has a profound effect on them, producing results similar to the biophysical data, indicating that this resistance must have changed upon entry into whole-cell mode. To see this figure in color, go online.

of increasing resistance (Fig. 5 *E*). A value between 100 and 300 MΩ was required to simulate our experimental observations. It should be noted that the possibility of an induced cross talk between recording and stimulating electrodes following patch rupture is ruled out, because in the salicylate-treated controls, no increase in tau is found following patch rupture.

Cable model

To hone in on the identity of the intervening resistance, R_{inter}, we assembled a 47 section cable model (Fig. 6 *A*) similar to the one devised by Halter et al. (11). We kept their basis values for R_L (0.001 mS/cm^2), R_{ecs}, R_{ax} (70 Ω cm), and R_{sc} (0.1 mS/cm^2); however, in our case we included lateral membrane NLC based on our measurements. Other values were R_s 10 MΩ, R_p 1.8 MΩ, R_{sh} 3–12 MΩ, C_m 0.8 μF/cm^2, C_b 3 pF, C_a 2pF, R_{mb} 300 MΩ, and R_{ma} 10 GΩ (high because stereocilia were damaged by trituration during cell isolation). ECS width was set to 30 nm. Similar to our experimental measures, a 10 kHz 4 pole Bessel filter implementation in Simulink was used on model currents.

As noted previously, we only observe single exponential current transients in our experiments. Fig. 6 *B* shows that the cable model cannot reproduce our data if we use the R_{sc} value of Halter et al. (11). The resultant pink solid lines are not simple single exponentials, and whole-cell NLC of this model (measured via the recording electrode) was substantially less than our biophysical measurements (Q_{max}: 1.35 pC vs. 2.95 pC). We must increase R_{sc} conductance by three orders of magnitude (0.15 S/cm^2) to fit our perforated patch data (*black solid lines*), and to simultaneously obtain a value matching our normal whole-cell NLC values (Q_{max}: 2.92 pC). This indicates that the SSC are highly conductive, on the order of electroporated membranes (23). To fit the data following patch rupture (Fig. 6 *C*), the ECS resistivity had to be increased three orders of magnitude (70 kΩ cm); this apparent increase in resistivity could instead indicate that the ECS space had collapsed or the actual ionic strength of the space had decreased. Additionally, R_{sc} conductance was reduced, as well (0.015 S/cm^2). Thus, the intervening resistance, R_{inter}, of the lumped parameter model corresponds to the R_{ecs} and R_{sc} components of the cable model. Fig. 7 shows time constants and NLC of the model using the perforated patch and whole-cell parameters obtained by trace fits. Similarity to the biophysical data is clear (compare with Fig. 2). These results

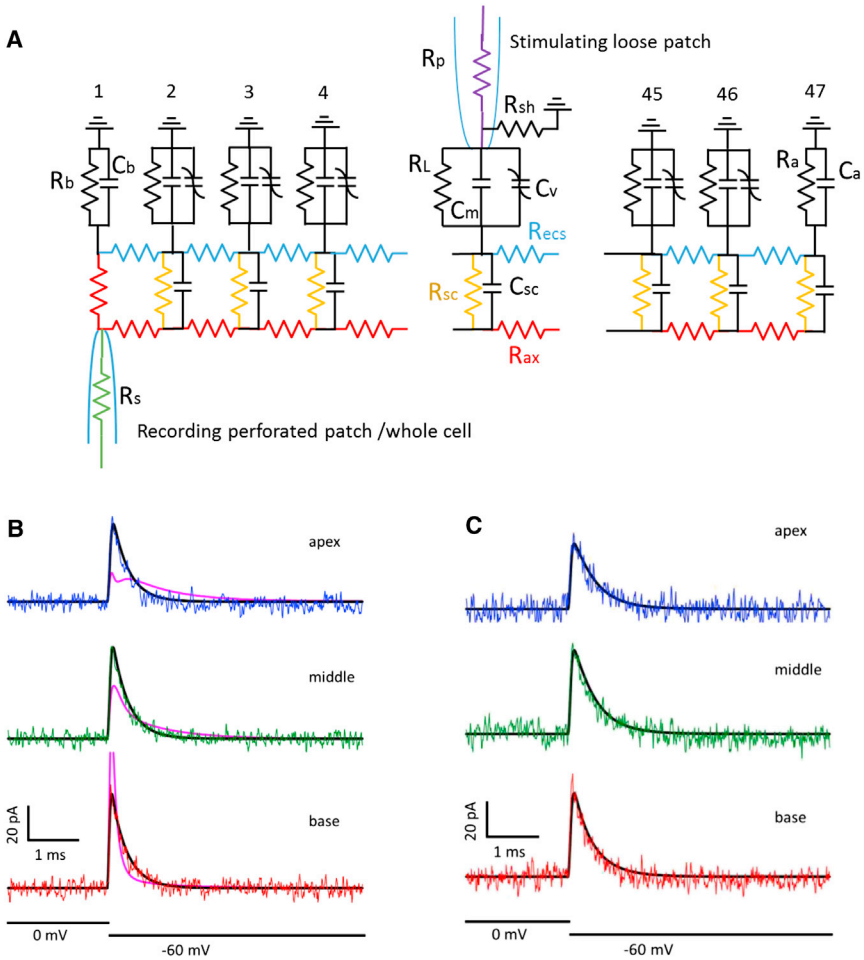

FIGURE 6 (*A*) Cable model with 47 sections. Roving loose patch electrode was placed at section 2, 22, and 42 to mimic basal, middle, and apical stimulations. See Model Results for parameter values. (*B*) R_{sc} values based on Halter et al. (11) (0.1 mS/cm^2) could not fit data in perforated mode (*pink traces*); however, a value of 0.15 S/cm^2 fit the data well (*black traces*). (*C*) For the model to fit whole-cell data, R_{ecs} resistivity had to be increased to 70 kΩ cm (*black traces*), with R_{sc} conductivity set to 0.015 S/cm^2. To see this figure in color, go online.

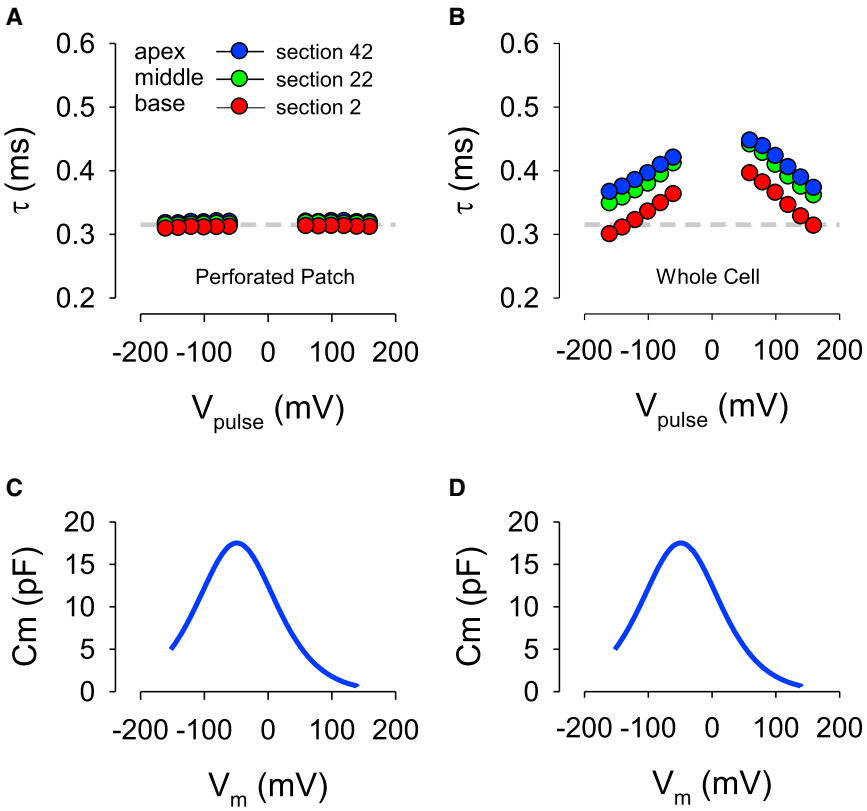

FIGURE 7 Cable model time constants (τ) of perforated (*A*) and whole-cell (*B*) patch responses induced by step voltages of the roving loose patch electrode. Note increase in time constants (τ) after change from perforated patch parameters to whole-cell parameters (see Model Results), and an apparent rise in voltage dependency similar to what is seen with the biophysical data. (*C*) and (*D*) show corresponding measures of whole-cell NLC measured with recording whole-cell electrode (Q_{max}, V_h, z: 2.78/2.94 pC, −40.7/−56.3 mV, 0.60/0.60). Compare to Fig. 2. To see this figure in color, go online.

indicate that under unperturbed conditions, with perforated patch recording intact, the high conductance of the SSC facilitates voltage delivery to the lateral membrane. Cable model results similar to the salicylate experiments were obtained with ECS resistivity set to 70 kΩ cm and R_{sc} conductivity of 0.03 or 0.026 S/cm^2 for perforated patch or whole-cell condition, respectively (model data not shown).

Finally, to evaluate the influence of SSC conductance on voltage excitation of the lateral membrane, we used our cable model driven by current injection into the cell's apical axial core, mimicking receptor currents (Fig. 8). In the absence of the SSC, frequency response magnitude is maximized, but phase is significantly changing at frequencies below 1 kHz. With R_{sc} conductivity from Halter et al. (11), significant reduction of frequency response magnitude and large phase changes across the spectrum arise. By increasing R_{sc} conductivity frequency response magnitude is enhanced and phase behavior is flattened. Thus, electrical transparency of the SSC tends to facilitate voltage delivery to the lateral membrane.

DISCUSSION

The mammalian OHC functions to enhance perception at acoustic frequencies, even beyond 100 kHz in some mammals. As a result, there is no doubt that the cell can produce mechanical activity at high frequencies (24), nor is there doubt that the OHC's stereocilia transduction apparatus operates at high frequencies (25–27). Indeed, there is little disagreement that cochlear amplification deriving from OHC electromechanics works most efficiently at high frequencies (28). Nevertheless the conundrum arising from a voltage-dependent basis of amplification continues to garner interest. The problem stems from the observed disparity between OHC resting membrane potential and the voltage where maximal mechanical activity occurs (V_h) (13,27). Should these two voltages overlap there would then be less difficulty with an RC filter. Several mechanisms have been postulated to understand why the RC filter should not interfere with prestin activity at high frequencies. Previously, we envisioned three mechanisms that might help: 1), because turgor pressure within the OHC shifts the voltage dependence of NLC and electromotility (22,29,30), we suggested that alterations in turgor pressure could align V_h and resting potential (22); 2), because prestin charge density increases in high-frequency OHCs (31,32), we reasoned that the rising electrical energy delivered to the lateral membrane could counter the reduced voltage drive; and 3), we reasoned that the flux of chloride through the stretch-activated chloride conductance, G_{metL}, in the lateral membrane could gate prestin's chloride-dependent activity independent of the membrane RC (6). Though the first two possibilities remain tenable, the latter is unlikely, because we have recently discovered that the effects of chloride on prestin are

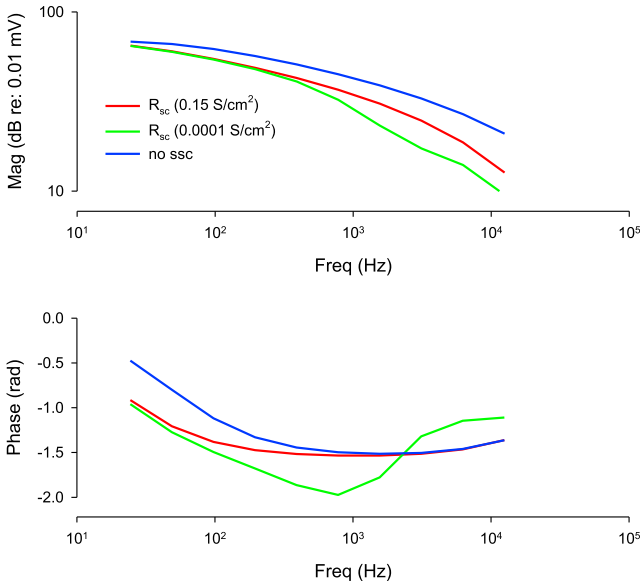

FIGURE 8 Magnitude and phase of voltage drop across section 33 lateral membrane of the cable model induced by 0.1 nA AC injection into the apical axial core. Without SSC frequency response is maximal. Reduction of R_{sc} from value based on Halter et al. (11) (0.1 mS/cm^2) tends to increase frequency response and provide a flat phase response. To see this figure in color, go online.

low-pass filtered by a slow intermediary state transition (33). Others, as well, have developed theories on overcoming the RC problem. These include 1), an intrinsic high pass augmentation of receptor potentials due to prestin's piezoelectricity (34); 2), a reduction of the RC effects by increases in membrane conductance (35); and 3), the observation that OHC resting potential may be more depolarized than the original estimates made in vivo (27,36), thus aligning resting potential and V_h (37).

Beyond the RC problem, however, ultrastructural specializations of the OHC lateral wall, namely the membranous SSC and the restricted, femtoliter space (ECS) it establishes, could provide isolation of the lateral membrane from axial receptor currents. This potentially could lead to reduced voltage drive to prestin motors embedded in the lateral membrane. Our present data directly relate to this issue.

Cable effects of the SSC

There has been a paucity of information on the electrical role of the SSC, mainly arising from modeling results of whole-cell electrical stimulation (11,38). Our experiments were aimed at electrically exploring restricted regions of the cell's lateral wall. Our data and model analyses indicate that the electrical transparency of the SSC promotes uniformly fast stimulus delivery to the lateral membrane motor, and therefore limits time-dependent, potentially nonlinear, activation of the motors. Based on average time to peak current measures between our apical and basal stimulus electrodes in the perforated patch condition (3.5 μs; see Results), for a 55 μm distance, a conduction velocity >150 m/s is obtained, and considering the high resistivity of the lateral plasma membrane, likely promotes isopotential conditions at any given acoustic frequency for the range of OHC lengths found within the cochlea spiral. This possibility was previously suggested because voltage-dependent conductances are absent along the OHC lateral membrane (21). The observation that damage to the SSC alters timing along the length of the OHC may indicate its high conductance is actively maintained. Indeed, the row of mitochondria adjacent to the SSC may play a role, because the washin of gramicidin following perforated patch rupture may uncouple mitochondrial oxidative phosphorylation (39). It is noteworthy that salicylate can also uncouple mitochondrial oxidative phosphorylation (40). We are currently evaluating the effects of other mitochondrial perturbations on SSC conductance.

Interestingly, in the model of Halter et al. (11), ECS current was found to exceed that within the cell's axial core, possibly pointing to unusual differences in resistivity between ECS and axial cytoplasm as also suggested by Farinelli et al. (38). Nakagawa and Brownell (12) have used the voltage-dependent dye, di-8-ANEPPS, to observe high frequency phase differences between OHC basal and lateral membrane voltages, which they attribute to the effects of a higher resistance of the axial core than ECS. Of course, this is counter intuitive based on the cross-sectional area of the ECS. Indeed, even fluorescent dye diffusion is somewhat slower in the ECS than in the axial core, though, of course, dye spread may not necessarily correlate with current spread (41). We were able to obtain single-exponential behavior of currents with our cable model if we set R_{ecs} resistivity to 0.7 Ω cm, while maintaining the higher R_{ax} resistivity at 70 Ω cm and R_{sc} conductivity at 0.1 mS/cm^2. However, typical values of cytosolic resistivity range between ~30 and 600 Ω cm (42), and considering the geometry of the ECS, this would mean that the ionic strength of the space would be enormous. It could be that the abundance of prestin within the lateral membrane, estimated to be up to 10 million copies based on nonlinear charge movement (43), contributes to a higher ionic strength in the ECS by virtue of its transport capabilities (44–46). Nevertheless, we consider it more reasonable to have the SSC highly conductive, possibly due to fenestrations, or vesiculations that may require work to maintain, because phospholipid bilayers tend to assume planar configurations (47). In this scenario, we might expect the performance of the OHC to be dependent on the energetics required to maintain an unusually high SSC conductivity.

ACKNOWLEDGMENTS

This research was supported by National Institutes of Health (NIH) National Institutes of Deafness and Other Communication Disorders (NIDCD) grant DC00273 to J.S.S.

REFERENCES

1. Ashmore, J., P. Avan, …, B. Canlon. 2010. The remarkable cochlear amplifier. *Hear. Res.* 266:1–17.
2. Holley, M. C., and J. F. Ashmore. 1988. A cytoskeletal spring in cochlear outer hair cells. *Nature.* 335:635–637.
3. Dieler, R., W. E. Shehata-Dieler, and W. E. Brownell. 1991. Concomitant salicylate-induced alterations of outer hair cell subsurface cisternae and electromotility. *J. Neurocytol.* 20:637–653.
4. Zheng, J., W. Shen, …, P. Dallos. 2000. Prestin is the motor protein of cochlear outer hair cells. *Nature.* 405:149–155.
5. Oliver, D., D. Z. He, …, B. Fakler. 2001. Intracellular anions as the voltage sensor of prestin, the outer hair cell motor protein. *Science.* 292:2340–2343.
6. Rybalchenko, V., and J. Santos-Sacchi. 2003. Cl- flux through a non-selective, stretch-sensitive conductance influences the outer hair cell motor of the guinea-pig. *J. Physiol.* 547:873–891.
7. Abe, T., S. Kakehata, …, H. Shinkawa. 2007. Developmental expression of the outer hair cell motor prestin in the mouse. *J. Membr. Biol.* 215:49–56.
8. Liberman, M. C., J. Gao, …, J. Zuo. 2002. Prestin is required for electromotility of the outer hair cell and for the cochlear amplifier. *Nature.* 419:300–304.
9. Santos-Sacchi, J. 1991. Reversible inhibition of voltage-dependent outer hair cell motility and capacitance. *J. Neurosci.* 11:3096–3110.
10. Ashmore, J. F. 1990. Forward and reverse transduction in the mammalian cochlea. *Neurosci. Res. Suppl.* 12:S39–S50.
11. Halter, J. A., R. P. Kruger, …, W. E. Brownell. 1997. The influence of the subsurface cisterna on the electrical properties of the outer hair cell. *Neuroreport.* 8:2517–2521.
12. Nakagawa, T., J. S. Oghalai, …, W. E. Brownell. 2006. Photometric recording of transmembrane potential in outer hair cells. *J. Neural Eng.* 3:79–86.
13. Santos-Sacchi, J. 1989. Asymmetry in voltage-dependent movements of isolated outer hair cells from the organ of Corti. *J. Neurosci.* 9:2954–2962.
14. Anson, B. D., and W. M. Roberts. 1998. A novel voltage clamp technique for mapping ionic currents from cultured skeletal myotubes. *Biophys. J.* 74:2963–2972.
15. Song, L., and J. Santos-Sacchi. 2010. Conformational state-dependent anion binding in prestin: evidence for allosteric modulation. *Biophys. J.* 98:371–376.
16. Santos-Sacchi, J., L. Song, …, A. L. Nuttall. 2006. Control of mammalian cochlear amplification by chloride anions. *J. Neurosci.* 26:3992–3998.
17. Santos-Sacchi, J., S. Kakehata, and S. Takahashi. 1998. Effects of membrane potential on the voltage dependence of motility-related charge in outer hair cells of the guinea-pig. *J. Physiol.* 510:225–235.
18. Kakehata, S., and J. Santos-Sacchi. 1996. Effects of salicylate and lanthanides on outer hair cell motility and associated gating charge. *J. Neurosci.* 16:4881–4889.
19. Tunstall, M. J., J. E. Gale, and J. F. Ashmore. 1995. Action of salicylate on membrane capacitance of outer hair cells from the guinea-pig cochlea. *J. Physiol.* 485:739–752.
20. Horn, R., and A. Marty. 1988. Muscarinic activation of ionic currents measured by a new whole-cell recording method. *J. Gen. Physiol.* 92:145–159.
21. Santos-Sacchi, J., G. J. Huang, and M. Wu. 1997. Mapping the distribution of outer hair cell voltage-dependent conductances by electrical amputation. *Biophys. J.* 73:1424–1429.
22. Kakehata, S., and J. Santos-Sacchi. 1995. Membrane tension directly shifts voltage dependence of outer hair cell motility and associated gating charge. *Biophys. J.* 68:2190–2197.
23. Hibino, M., M. Shigemori, …, K. Kinosita, Jr. 1991. Membrane conductance of an electroporated cell analyzed by submicrosecond imaging of transmembrane potential. *Biophys. J.* 59:209–220.
24. Frank, G., W. Hemmert, and A. W. Gummer. 1999. Limiting dynamics of high-frequency electromechanical transduction of outer hair cells. *Proc. Natl. Acad. Sci. USA.* 96:4420–4425.
25. Dallos, P. 1985. Membrane potential and response changes in mammalian cochlear hair cells during intracellular recording. *J. Neurosci.* 5:1609–1615.
26. Russell, I. J., A. R. Cody, and G. P. Richardson. 1986. The responses of inner and outer hair cells in the basal turn of the guinea-pig cochlea and in the mouse cochlea grown in vitro. *Hear. Res.* 22:199–216.
27. Dallos, P., J. Santos-Sacchi, and A. Flock. 1982. Intracellular recordings from cochlear outer hair cells. *Science.* 218:582–584.
28. Ruggero, M. A., and N. C. Rich. 1991. Furosemide alters organ of corti mechanics: evidence for feedback of outer hair cells upon the basilar membrane. *J. Neurosci.* 11:1057–1067.
29. Iwasa, K. H. 1993. Effect of stress on the membrane capacitance of the auditory outer hair cell. *Biophys. J.* 65:492–498.
30. Gale, J. E., and J. F. Ashmore. 1994. Charge displacement induced by rapid stretch in the basolateral membrane of the guinea-pig outer hair cell. *Proc. Biol. Sci.* 255:243–249.
31. Santos-Sacchi, J., S. Kakehata, …, T. Takasaka. 1998. Density of motility-related charge in the outer hair cell of the guinea pig is inversely related to best frequency. *Neurosci. Lett.* 256:155–158.
32. Corbitt, C., F. Farinelli, …, B. Farrell. 2012. Tonotopic relationships reveal the charge density varies along the lateral wall of outer hair cells. *Biophys. J.* 102:2715–2724.
33. Song, L., and J. Santos-Sacchi. 2013. Disparities in voltage-sensor charge and electromotility imply slow chloride-driven state transitions in the solute carrier SLC26a5. *Proc. Natl. Acad. Sci. USA.* 110:3883–3888.
34. Spector, A. A., W. E. Brownell, and A. S. Popel. 2003. Effect of outer hair cell piezoelectricity on high-frequency receptor potentials. *J. Acoust. Soc. Am.* 113:453–461.
35. Ospeck, M., X. X. Dong, …, K. H. Iwasa. 2006. Electromotility in outer hair cells: a supporting role for fast potassium conductance. *ORL J. Otorhinolaryngol. Relat. Spec.* 68:373–377.
36. Russell, I. J., and P. M. Sellick. 1983. Low-frequency characteristics of intracellularly recorded receptor potentials in guinea-pig cochlear hair cells. *J. Physiol.* 338:179–206.
37. Johnson, S. L., M. Beurg, …, R. Fettiplace. 2011. Prestin-driven cochlear amplification is not limited by the outer hair cell membrane time constant. *Neuron.* 70:1143–1154.
38. Farinelli, F., W. Brownell, and B. Farrell. 2010. Evidence that the subsurface cisternae influences the electrical properties of the outer hair cell. Abstracts of the Thirty-Third Annual Midwinter Research Meeting. *Assoc. Res. Otolaryngol.* 33:194–195, Abstract 571.
39. Rottenberg, H., and R. E. Koeppe, 2nd. 1989. Stimulation of cation transport in mitochondria by gramicidin and truncated derivatives. *Biochemistry.* 28:4361–4367.
40. Miyahara, J. T., and R. Karler. 1965. Effect of salicylate on oxidative phosphorylation and respiration of mitochondrial fragments. *Biochem. J.* 97:194–198.
41. Ashmore, J., and J. Gale. 2004. The cochlear amplifier. *Curr. Biol.* 14:R403–R404.
42. Golding, N. L., T. J. Mickus, …, N. Spruston. 2005. Factors mediating powerful voltage attenuation along CA1 pyramidal neuron dendrites. *J. Physiol.* 568:69–82.
43. Huang, G., and J. Santos-Sacchi. 1993. Mapping the distribution of the outer hair cell motility voltage sensor by electrical amputation. *Biophys. J.* 65:2228–2236.
44. Bian, S. M., B. W. Koo, …, D. Navaratnam. 2011. Evaluating prestin's changing biophysical attributes in development using a tet-induced cell

line. What fire is in mine ears. *Progress in Auditory Biomechanics.* 1403:143–147.

45. Bai, J. P., A. Surguchev, …, D. Navaratnam. 2009. Prestin's anion transport and voltage-sensing capabilities are independent. *Biophys. J.* 96:3179–3186.

46. Mistrík, P., N. Daudet, …, J. F. Ashmore. 2012. Mammalian prestin is a weak Cl^-/HCO_3^- electrogenic antiporter. *J. Physiol.* 590:5597–5610.

47. Graham, T. R., and M. M. Kozlov. 2010. Interplay of proteins and lipids in generating membrane curvature. *Curr. Opin. Cell Biol.* 22:430–436.